PAPER

Check for updates

On the lack of monoclinic distortion in the insulating regime of EuNiO₃ and GdNiO₃ perovskites by high-angular resolution synchrotron X-ray diffraction: a comparison with YNiO₃†

Federico Serrano-Sánchez, [ID] [a] José Luis Martínez, [ID] [a] François Fauth [ID] [b] and José Antonio Alonso [ID] *[a]

Rare-earth nickelates RNiO₃ (R = Y, La⋯Lu) are electron-correlated perovskite materials where the interplay between charge and spin order results in a rich phase diagram, evolving from antiferromagnetic insulators to paramagnetic metals. They are well-known to undergo metal–insulator (MI) transitions as a function of temperature and the size of the rare-earth ion. For intermediate-size Eu^{3+} and Gd^{3+} ions, the MI transitions are described to happen at T_{MI} = 463 K and 511 K, respectively. We have investigated their structural evolution across T_{MI} with the excellent angular resolution of synchrotron X-ray diffraction, using high-crystalline quality samples prepared at elevated hydrostatic pressures. Unlike YNiO₃, synthesized and measured under the same conditions, exhibiting a characteristic monoclinic phase (space group $P2_1/n$) in the insulating regime (below T_{MI}), the present EuNiO₃ and GdNiO₃ samples do not exhibit such a symmetry, but their crystal structures can be defined in an orthorhombic superstructure of perovskite (space group *Pbnm*) in all the temperature interval, between 100 and 623 K for Eu and 298 K and 650 K for Gd. Nevertheless, an abrupt evolution of the unit-cell parameters is observed upon metallization above T_{MI}. A prior report of a charge disproportionation effect by Mössbauer spectroscopy on Fe-doped perovskite samples seems to suggest that the distribution of two distinct Ni sites must not exhibit the required long-range ordering to be effectively detected by diffraction methods. An abrupt contraction of the *b* parameter of EuNiO₃ in the 175–200 K range, coincident with the onset of antiferromagnetic ordering, suggests a magnetoelastic coupling, not described so far in rare-earth nickelates. The magnetic susceptibility is dominated by the paramagnetic signal of the rare-earth ions; however, the AC susceptibility curves yield a Néel temperature corresponding to the antiferromagnetic ordering of the Ni moments of T_N = 197 K for EuNiO₃, corroborated by specific heat measurements. For GdNiO₃, a χT vs. T plot presents a clear change in the slope at T_N = 187 K, also consistent with specific heat data. Magnetization measurements at 2 K under large fields up to 14 T show a complete saturation of the magnetic moments with a rather high ordered moment of 7.5μB per f.u.

Introduction

Complex transition-metal oxides display a striking range of relevant phenomena, such as unconventional quantum magnetic transitions, colossal magnetoresistance, ionic conduction and superconductivity.[1–3] Among them, electronic correlations and interplay of charge and spin order in RNiO₃ perovskites result in a rich phase diagram, from antiferromagnetic insulators to paramagnetic metals, holding a great interest for the scientific community.[4–9]

The high-temperature *Pbnm* orthorhombic structure of RNiO₃ (R = Pr → Lu) perovskites undergoes a reversible metallic to insulator (MI) transition, the temperature of which (T_{MI}) increases along the rare earth series from PrNiO₃ (T_{MI} = 130 K) to LuNiO₃ (T_{MI} = 600 K). The LaNiO₃ system behaves differently, as it displays a rhombohedral *R-3c* structure and solely a metallic behavior. This behavior is driven by the overlap of the Ni (3d) and O (2p) orbitals depending on R^{3+} cationic radius, which determines the p–d Ni–O bond length and octahedral Ni–Ô–Ni tilting angle.[5,9] The structural parameters define the tolerance factor of the perovskite as $t = d_{R–O}/\sqrt{2}d_{Ni–O}$, which

[a]Instituto de Ciencia de Materiales de Madrid (ICMM), Consejo Superior de Investigaciones Científicas (CSIC), Sor Juana Inés de la Cruz 3, E-28049 Madrid, Spain. E-mail: ja.alonso@icmm.csic.es
[b]CELLS–ALBA Synchrotron, Cerdanyola del Valles, Barcelona, E-08290 Spain
†Electronic supplementary information (ESI) available. See DOI: 10.1039/d1dt00646k

has shown to be a determining factor of the valence bandwidth, and thus, the MI transition and magnetic behavior.

After thorough experimental and theoretical investigations, the exact mechanisms underlying the MI transition are still under discussion.[10] Initially, the electronic localization was explained by a charge disproportionation into two different Ni sites as $Ni^{3+} \rightarrow Ni^{(3-\delta)+} + Ni^{(3+\delta)+}$ through the transition to the insulating regime.[4,11–15] In this regime, the perovskite structure displays large and small octahedra with different average Ni–O bond lengths, which is realized in a monoclinic crystal structure defined in the $P2_1/n$ space group. This is described as a breathing-like distortion in which the charge disproportionation removes the Ni electronic state degeneracy, opening a band gap. More recently, another related description places positive charges in the oxygen p-orbitals, with the electronic configuration of Ni^{2+} $3d^8L$ in the metallic state and $3d^8L^2 + 3d^8$ in the insulating phase, with L denoting a positive charge held by the oxygen ligands, leaving the Ni valence state virtually the same in both octahedra.[13,16,17] This explanation is named bond disproportionation and is based on the strong covalent character of the Ni–O bonds and the major contribution of the oxygen p-orbitals to the valence band top. Both descriptions include the distortion of the NiO_6 octahedra and a charge rearrangement within the structure. Bond disproportionation has proven to be a good physical description to capture the basic properties using theoretical approaches,[18] while many studies have reported experimental proof of the differently charged octahedral environment in the whole $RNiO_3$ series, using X-ray absorption spectroscopy (XAS),[19] Resonant X-Ray scattering,[20] and Raman[21] and Mössbauer spectroscopy.[14] Moreover, similar electronic and magnetic structures have been observed for the series by soft X-ray magnetic diffraction,[22] indicating the analogous behavior of the insulating phase.

The antiferromagnetic ordering at low temperature is also dependent on the size of R^{3+} cations as the Néel temperature T_N is simultaneous with the MI transition for large R cations (R = Pr–Nd), while for the rest of the series (R = Sm–Lu), T_N is well below T_{MI}. This indicates that the MI transition is not associated with the onset of AF ordering. On the other hand, the occurrence of noticeable ^{16}O–^{18}O isotope shifts of T_{MI} in $RNiO_3$ (R = Pr, Nd, Sm and Eu) establishes the significance of electron–lattice coupling in these oxides.[23] Soft X-ray and magnetic neutron diffraction experiments have described a non-collinear stacking of alternate up–up–down–down Ni spins along the propagation vector $k = (1/2, 0, 1/2)$.[22,24] Furthermore, magnetic rare-earth elements may display long-range ordering, as in $HoNiO_3$.[25]

In the small $RNiO_3$ (R = Y, Dy → Lu) derivatives, a structural transition accompanying the MI transition has been described by neutron and high-angular resolution X-ray diffraction. As mentioned, the orthorhombic high-temperature structure distorts into a monoclinic $P2_1n$ structure,[4,11,12,15,26,27] yielding the two differentiated Ni octahedra with long-range periodic order described as a breathing distortion. The experimental observations of the charge disproportionation suggest that this dis-

tortion is present in the insulating phase of the whole rare earth series.[22] However, for larger $RNiO_3$ (R = Pr → Gd), the structural transition had not been identified.

The metastable character of $EuNiO_3$ has made it difficult to investigate.[3,6,28] It presents a clear gap between the MI (T_{MI} = 463 K) and antiferromagnetic transition (T_N = 220 K). Neither the low temperature phase structure nor the magnetic properties of this compound have been reported. $GdNiO_3$ has been studied and prepared under high O_2 pressure conditions, showing no signs of monoclinic distortion below T_{MI} = 510 K, with T_N = 185 K.[7] Besides, a large absorption cross section of Eu and Gd makes difficult any neutron diffraction characterization.

Recently, we described the structural transition to the monoclinic phase of $SmNiO_3$, owing to an excellent crystallinity of the samples prepared at 3.5 GPa under oxidizing conditions, combined with high-angular resolution diffraction experiments.[29] These allowed us to identify a monoclinic insulating phase and the subtle changes in the crystal structure across the transition. In the present study, an identical high-pressure preparation (3.5 GPa) of pure $EuNiO_3$ and $GdNiO_3$ perovskites is reported, along with a detailed diffraction study of the crystalline structure above and below the T_{MI} using high-angular resolution synchrotron X-ray diffraction. Even though the monoclinic structure is not observed, a sharp variation of the structural parameters occurs at T_{MI}. This indicates that the charge disproportionation preliminary observed by Mössbauer spectroscopy[31,32] is a local phenomenon and there is no long-range order of the NiO_6 octahedra. This structural study is complemented with the examination under the same diffraction conditions of $YNiO_3$, providing with a reference of a compound that indeed experiences an orthorhombic-to-monoclinic transition across T_{MI}. Finally, the susceptibility and heat capacity measurements of $GdNiO_3$ and $EuNiO_3$ perovskites are reported, showing for the first time some anomalies at the thermal evolution of the structural parameters of the Eu compound across T_N, suggesting a magneto-elastic behavior.

Experimental section

$EuNiO_3$, $GdNiO_3$ and $YNiO_3$, were synthesized under identical high-pressure (HP) conditions. Stoichiometric mixtures of Ni $(OH)_2$, and Eu_2O_3 or Gd_2O_3 or Y_2O_3 (of analytical grade) were ground in an agate mortar with 30% $KClO_4$, incorporated to provide an "in situ" high oxygen pressure to promote the oxidation of nickel to Ni^{3+}. The precursor mixture was introduced into a gold capsule of 5 mm diameter and set within a cylindrical graphite heater serving as heater element. A hydrostatic pressure of 3.5 GPa was applied using a piston-cylinder Rockland Research press; the sample was then heated at 900 °C for 20 min, followed by quenching. The KCl resulting from the decomposition of $KClO_4$ and traces of R_2O_3 and NiO were subsequently eliminated by washing the resulting powder in a diluted HNO_3 solution at 60 °C. The sample was then dried at 150 °C for 1 h in air.

The nature of the resulting powder was assessed by laboratory X-ray diffraction (XRD) using a Bruker-AXS D8 diffractometer (40 kV, 30 mA), with Cu Kα radiation (λ = 1.5418 Å). The Synchrotron X-ray diffraction (SXRD) experiments were carried out in the transmission mode on the BL04-MSPD beamline of the ALBA synchrotron (Barcelona, Spain) using the highest angular resolution mode as provided by the MAD setup.[30] The $RNiO_3$ oxides were sealed in 0.7 mm diameter quartz capillaries that were rotating during the acquisition time to increase powder averaging. The beam energy was 28 keV (λ = 0.4427 Å) for R = Gd and Y and 32 keV (λ = 0.38776 Å) for R = Eu, selected to minimize absorption. Room temperature (RT, 298 K) patterns were collected for the three samples; then sequential SXRD patterns were collected at 100, 150, 200, 250, 295, 350, 373, 423, 448, 473, 498, 523, 573 and 623 K for $EuNiO_3$ and 298, 400, 450, 277, 550 and 650 K for $GdNiO_3$.

The analysis of the SXRD data was performed by the Rietveld method, using the FullProf Suite. The diffraction peak shape was defined by a pseudo-Voight function; a linear interpolation between points devoid of reflections was considered as the background. The final refinement included the scale factor, zero-point shift, width and asymmetry parameters, unit-cell parameters, atomic positions and isotropic displacement factors. No regions were excluded from the refinements.

Magnetic susceptibility was measured using a SQUID Magnetometer from Quantum Design (QD, USA) model MPMS-XL in the range of 1.8 K to 400 K and magnetic fields up to 5 T. Complementary data on magnetization at high magnetic fields (14 T) and AC magnetic susceptibility were performed in using the VSM and AC options of the PPMS system from QD. Heat capacity measurements in the range 1.8 K to 300 K at different applied external magnetic fields (up to 9 T) were measured using the PPMS system with a heat pulse method.

Results and discussion

Structural characterization

$EuNiO_3$, $GdNiO_3$ and $YNiO_3$ nickelates were successfully prepared under a high hydrostatic pressure of 3.5 GPa in the presence of $KClO_4$. $YNiO_3$ has been previously characterized by neutron diffraction[4,11] and a charge disproportionation effect described in the monoclinic $P2_1/n$ (#15) space group was reported for the first time for this compound; here it is used as a reference oxide. $EuNiO_3$ and $GdNiO_3$ had also been previously reported from a synthetic procedure involving a high-oxygen pressure of 200 bar,[6,7] and described at RT in an orthorhombic superstructure of perovskite (space group *Pbnm*, #62). However, a further study by neutron diffraction could not be realized given the absorbing nature of both the Eu and Gd elements. Neutrons are essential to discriminate the subtle shifts of the oxygen atoms associated with the charge disproportionation effect, but SXRD data are also capable of detecting the subtle monoclinic distortions related to this electronic

effect, and therefore, to unveil any deviation from the orthorhombic symmetry. The present preparation procedure, involving the treatment of $Ni(OH)_2$ and R_2O_3 mixtures together with $KClO_4$, at 3.5 GPa and 800 °C, provides much better crystallized samples, which translates in narrower peaks, where the suitable high-resolution diffraction studies indeed assess the true symmetry of these materials and its evolution with temperature.

For $YNiO_3$, the RT SXRD pattern clearly enables the visualization of typical reflection splitting suggesting a monoclinic symmetry. Fig. 1a shows the characteristic (−224)/(224) splitting observed in $YNiO_3$, where these two peaks are perfectly resolved, whereas for $GdNiO_3$ a single peak is observed for this reflection. As a reference, the subtle splitting recently described for $SmNiO_3$[29] is also included in the figure; these three samples were collected with the same wavelength (λ = 0.4427 Å).
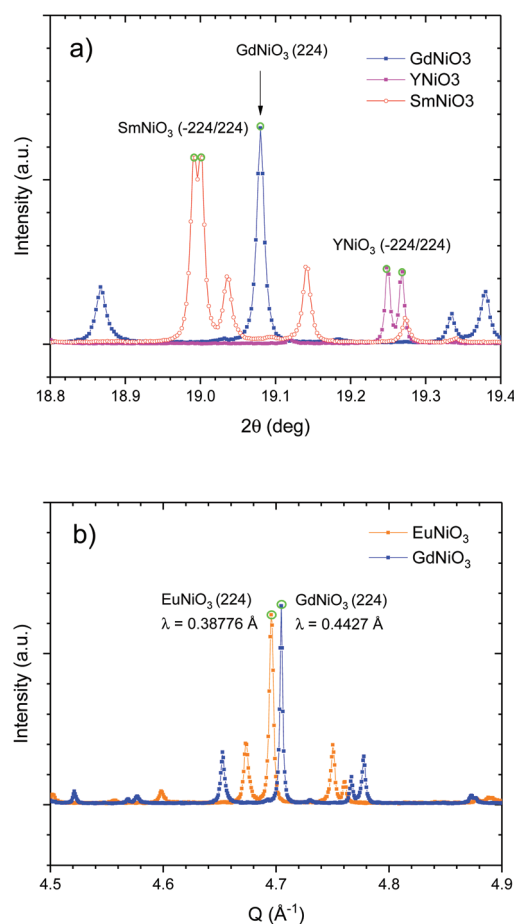
Fig. 1 (a) Characteristic splitting (−224)/(224) observed for $YNiO_3$ at RT shown in a region of the SXRD patterns of $YNiO_3$ and $GdNiO_3$ as a function of 2θ, in comparison with that detected for $SmNiO_3$ (from ref. 29), and the absence of splitting experienced by $GdNiO_3$ for the same reflection. b) Selected region of the SXRD patterns of $EuNiO_3$ and $GdNiO_3$ represented as a function of Q (Å^{-1}), highlighting the (224) reflection, illustrating a similar width and the absence of the splitting characteristic of the monoclinic symmetry.

A second related figure (Fig. 1b) is necessary to include together the data of GdNiO$_3$ and EuNiO$_3$, since this last pattern was collected at a different energy and wavelength (λ = 0.38776 Å); in this figure a representation as a function of Q (Å^{-1}) is utilized. Fig. 2 shows that the characteristic (224) reflection is not apparently split, and a comparable peak width manifesting a similar degree of crystallization is observed.

In consequence, while for YNiO$_3$ the refinement of the crystal structure from the SXRD data at RT (in the insulating regime) was performed in the monoclinic space group $P2_1/n$, as previously reported from the neutron data,[4,11] the preliminary trials in the mentioned symmetry for EuNiO$_3$ and GdNiO$_3$ were unsuccessful, yielding almost negligible monoclinic distortions (monoclinic β angles below 90.01°) and negative thermal factors for some Ni or oxygen atoms. Therefore, the orthorhombic space group $Pbnm$ was considered at RT for EuNiO$_3$ and GdNiO$_3$. Fig. 2 shows the diffraction patterns after the Rietveld fit at room temperature for these two samples. As mentioned, for YNiO$_3$ the excellent crystallinity together with the outstanding angular resolution of MSPD diffractometer yielded extremely narrow peaks (half-maximum width of typically F_{WHM} = 0.01° at 12° 2θ), which were essential to discern the structural distortion associated with the charge disproportionation effect in this case. Therefore, only for YNiO$_3$ at RT the superstructure of perovskite is defined in the monoclinic space group $P2_1/n$, with unit-cell parameters related to that of the aristotype a_0 as $a_0 \approx \sqrt{2}a_0$, $b \approx \sqrt{2}a_0$ and $c \approx 2a_0$. This model contains two different Ni atoms, Ni1 and Ni2, located at 2d and 2c sites, respectively, and three O atoms, O1, O2 and

O3, located at the 4e general crystallographic positions. The structural parameters are detailed at the ESI in Table S1.† The Rietveld plot for YNiO$_3$ at RT is also included in the ESI as Fig. S1.† The same attributes regarding the crystallinity and resolution (F_{WHM} = 0.01° at 12° 2θ) also helped to demonstrate that EuNiO$_3$ and GdNiO$_3$ must be described as orthorhombic at RT.

In the orthorhombic model utilized to refine the structure for the Eu and Gd counterparts at RT, defined in the $Pbnm$ space group, there is a unique Ni atom at 4b positions and two O1 and O2 atoms at 4c and 8b Wyckoff sites, respectively; Eu and Gd are also located at 4c sites. The structural parameters at RT are included in Table 1.

The thermal evolution of the structural parameters of EuNiO$_3$ and GdNiO$_3$ has been studied across the metal-to-insulator transition (Fig. 3 and 4). In the case of Eu, the SXRD data could also be collected below RT, across the antiferromagnetic-ordering transition, occurring at T_N = 220 K.[28] The crystal structure for both compounds was refined in the orthorhombic crystallographic model in all the temperature interval. Fig. 3 illustrates the goodness of the fit for the high-temperature patterns, e.g. 623 K for EuNiO$_3$ and 650 K for GdNiO$_3$. Fig. 3a shows that, for EuNiO$_3$, the a unit-cell parameter steadily increases for the whole temperature range 100–600 K, while b experiences a non-monotonic evolution with two anomalies: the former at about 175–200 K, coincident with the magnetic ordering temperature, and the second anomaly includes an abrupt contraction and, then, an expansion, concomitant with the MI transition, happening at T_{MI} = 463 K.[6]

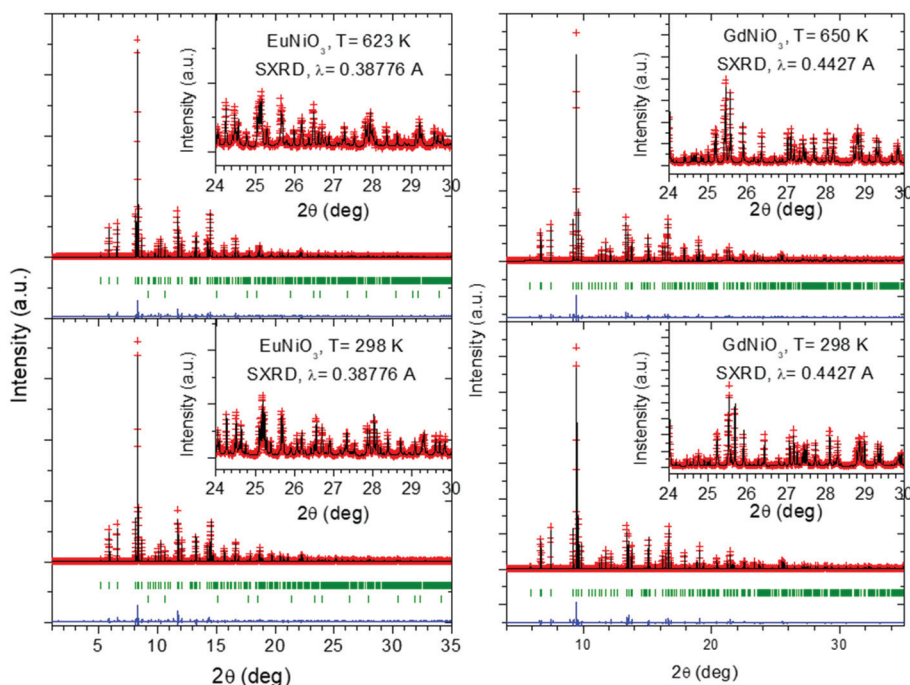**Fig. 2** Rietveld plots from the SXRD data of EuNiO$_3$ (left column) at RT and 623 K and GdNiO$_3$ (right column, at RT and 650 K), corresponding to the structural refinements in the orthorhombic $Pbnm$ space group in all cases. The insets show a close up of the high-angle region, highlighting the quality of the fit. The second series of Bragg reflections for EuNiO$_3$ correspond to a minor impurity of NiO.

Table 1 Structural parameters of $EuNiO_3$ and $GdNiO_3$ in the space group $P2_1/n$ at RT, below and above the MI transition, determined by SXRD

| $EuNiO_3$ $Pbnm$				$GdNiO_3$ $Pbnm$	
Temperature (K)	100	300	623	303	650
a (Å)	5.28107(3)	5.29060(3)	5.31271(4)	5.25967	5.28467(2)
b (Å)	5.46653(3)	5.46506(3)	5.46064(4)	5.49015	5.49062(2)
c (Å)	7.52227(4)	7.53586(5)	7.55499(5)	7.51213	7.53257(3)
V (Å^3)	217.161(2)	217.888(2)	219.176(3)	216.923(1)	218.566(1)
R 4c ($x\ y\ \frac{1}{4}$)					
x	0.9865(2)	0.9870(2)	0.9882(2)	0.9852(1)	0.9861(1)
y	0.0596(1)	0.0584(2)	0.0551(2)	0.0631(1)	0.0602(1)
B_{iso} (Å^2)	0.38 (2)	0.60(2)	0.99(2)	0.26(1)	0.73(1)
O1 4c ($x\ y\ \frac{1}{4}$)					
X	0.083(2)	0.082(3)	0.078(2)	0.087(2)	0.086(2)
Y	0.478(2)	0.480(2)	0.478(2)	0.475(1)	0.476(2)
B_{iso} (Å^2)	0.61(2)	1.1 (3)	1.7(3)	0.1(2)	0.8(2)
O2 8d ($x\ y\ z$)					
x	0.705(1)	0.705(2)	0.708(2)	0.700(1)	0.704(1)
y	0.295(1)	0.297(2)	0.301(2)	0.297(1)	0.299(1)
z	0.0468(9)	0.046(1)	0.045(1)	0.0466(9)	0.0445(8)
B_{iso} (Å^2)	0.02(20)	0.1(1)	0.1(2)	0.5(1)	0.5(1)
Ni1 4b ($\frac{1}{2}\ 0\ 0$)					
B_{iso} (Å^2)	0.37(4)	0.52(4)	0.64(4)	0.25(3)	0.52(3)
Reliability factors					
R_I (%)	6.11	5.97	5.97	3.82	3.67
R_p (%)	15.4	15.2	16.6	12.7	12.1
R_{wp} (%)	21.5	20.5	21.1	16.0	14.8
R_{exp} (%)	8.94	9.22	9.55	7.47	8.09
χ^2	5.79	4.95	4.87	4.59	3.36
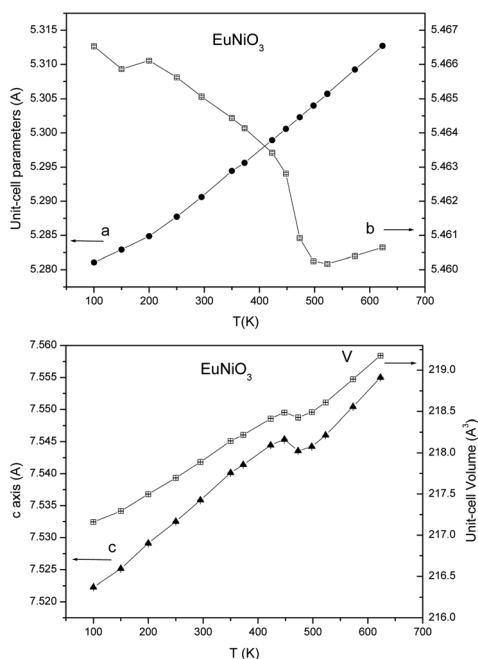
Fig. 3 Thermal evolution of the unit-cell parameters and unit-cell volume across the metal insulator transition (T_{MI} = 463 K) for $EuNiO_3$. An anomaly is observed in a parameter across T_N, where abrupt variations are observed in b and c upon entering the orthorhombic, metallic phase. The errors are smaller than the size of the symbols.
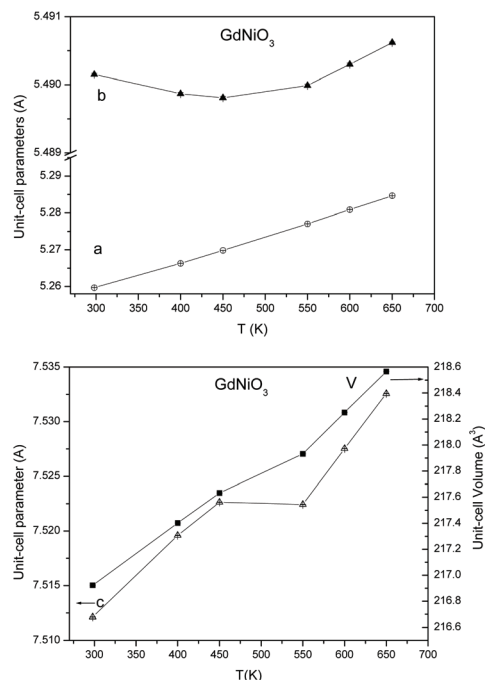
Fig. 4 Thermal evolution of the unit-cell parameters and unit-cell volume across the metal insulator transition (T_{MI} = 510 K) for $GdNiO_3$. An interruption of the thermal expansion is observed in c upon entering the orthorhombic, metallic phase. The errors are smaller than the size of the symbols.

Fig. 3c displays a similar contraction and then expansion of the c axis at the same characteristic temperature, across the phase transition upon entering the metallic regime. As a result

of that evolution, the volume also exhibits a characteristic contraction; the calculated superimposed volume contraction is $\Delta V/V = 0.12\%$, which is of the same order of magnitude as

those observed for other rare-earth nickelates upon metallization. For $GdNiO_3$, a less detailed temperature-dependent data collection could be performed, but basically the same overall evolution of the unit-cell parameters across the MI transition (T_{MI} = 511 K (ref. 7)) is observed, as illustrated in Fig. 4; the continuous expansion of the a parameter is accompanied by a non-monotonic contraction and then expansion in b and c parameters, as well as the unit-cell volume.

Therefore, we have verified by high-angular resolution diffraction tools that $EuNiO_3$ and $GdNiO_3$, prepared under the same high-pressure conditions as those of $YNiO_3$ and $SmNiO_3$[29] and exhibiting a comparable degree of crystallinity (as evaluated by the similar width of the diffraction peaks), do not offer evidence of a monoclinic distortion below T_{MI}, in the insulating region, unlike those previously observed for $SmNiO_3$,[29] $YNiO_3$[4,11,12] and other small rare-earth nickelates.[4,12,27] This is in contrast with the previous results of Mössbauer spectroscopy of ^{57}Fe-doped samples of $EuNiO_3$ and $GdNiO_3$, yielding evidence of the existence of two different environments for Fe, from what it was concluded that a charge disproportionation effect at the Ni sites was active in the insulation phases of these perovskites.[31,32] This result is, of course, an indirect evidence for the existence of two types of nickel positions in the insulating state of nickelate $RNiO_3$ lattices.[32] The present results, clearly indicating that an orthorhombic symmetry must be considered in all the temperature range, seem to suggest that the distribution of two distinct Ni sites must not exhibit the required long-range ordering to be effectively detected by diffraction methods. In these Fe-doped samples, it is conceivable that the two Fe sites, and therefore the Ni sites to which they replace, could be distributed at random within the crystallographic lattice, not providing with the essential coherence to unveil the characteristic features (either at the unit-cell parameters, and namely the monoclinic beta angle, as well as the internal symmetry necessary to define two distinct environments for Ni atoms) of an ordered charge-disproportionated state. The reason why $EuNiO_3$ and $GdNiO_3$ exhibit the proposed disordered charge disproportionation, while the neighboring $SmNiO_3$ perovskite is ordered, is uncertain, although it could be related to the nature of the rare-earth ion.

It is certainly remarkable that both $GdNiO_3$ and $EuNiO_3$, placed at the middle of the rare-earth series, exhibit a distinct behavior concerning the absence of long-range ordering detectable by diffraction methods. For Gd^{3+}, the 4f orbitals are half-filled ($4f^7$ configuration), hence particularly stable. As such, f–f transitions are not possible (this is the reason why this ion does not absorb any wavelength, and hence it is colourless). At the same time, Gd^{3+} is strongly paramagnetic, and the anisotropic nature of the Gd–Gd interactions may account for a homogeneous molecular field on the Ni sites. It is undeniable that the local molecular field of the rare-earth ions on neighboring Ni atoms may be of importance in the establishment or absence of long-range ordering between NiO_6 octahedra. Regarding Eu^{3+}, it is also well-known that Eu^{2+} is more stable than Eu^{3+} because of the magic configuration $4f^7$.[7]

Therefore, we cannot exclude some admixture with Eu^{2+}, isoelectronic with Gd^{3+}, and hence, the same considerations regarding the isotropic molecular field on neighbouring Ni ions and the absence of long-range ordering of the $Ni^{3+\delta}$ and $Ni^{3-\delta}$ octahedra could also apply here.

Magnetic properties

The magnetic susceptibility *vs.* *T* plot for $EuNiO_3$ is displayed in Fig. 5. This curve does not show any special anomaly around the antiferromagnetic ordering temperature (T_N), corresponding to the interactions between Ni spins, but only a broad maximum in the range 50 K to 250 K, with a final upward of the susceptibility below 50 K. This shows that the magnetism is dominated by the contribution of Eu to the susceptibility. The expected T_N for $EuNiO_3$ from the classical phase diagram Fig. 5, presented in the literature by Torrance *et al.*[9] is close to 205 K. This was determined in $EuNiO_3$ samples prepared under 200 bar O_2 pressure, from the paramagnetic fraction from muon-spin-rotation experiments, which drops suddenly at the antiferromagnetic ordering temperature. Alternatively, from NPD experiments in $^{153}EuNiO_3$, a T_N of 220 K was determined.[24] The lower inset of Fig. 5 shows the inverse magnetic susceptibility in the paramagnetic regime, which presents a perfect linear behavior corresponding to a paramagnetic moment of $5.5\mu_B$ per f.u.; this paramagnetic moment comes from both Ni and Eu ions. The Weiss temperature exhibits a value of θ = −326 K, indicating strong antiferromagnetic interactions in this paramagnetic temperature range.

Among the rare earth ions, most of them stabilize the R^{3+} valence state, with the corresponding paramagnetic moment. The case of Eu is usually special, because the most stable valence state is Eu^{2+}, with $J = S = 7/2$ and the magnetic moment is close to $7\mu_B$. Formally, the Eu^{3+} ($J = 0$) ion in principle does not carry any magnetic moment. In the practice, however, the paramagnetic moment of Eu^{3+} is reported to be

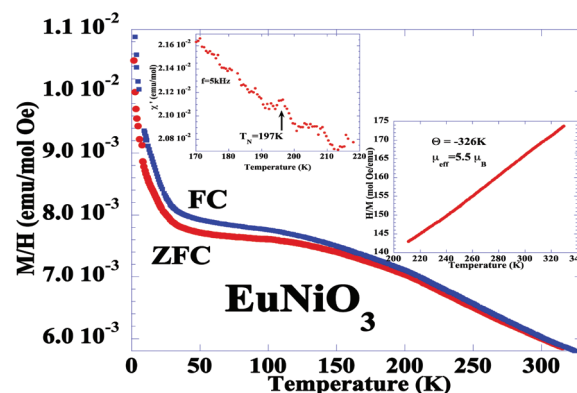**Fig. 5** Temperature dependence of the magnetic susceptibility of $EuNiO_3$. The upper inset shows the AC magnetic susceptibility at 5 kHz frequency with a weak peak around T_N = 197 K. The lower inset shows the inverse magnetic susceptibility well above T_N, indicating a paramagnetic linear behavior.

close to $3.4\mu_B$. In our case, we estimate that the valence state is Eu^{3+}; however, probably due to the local electrical and magnetic fields coming from the Ni sublattice, the J levels possibly undergo a complex admixture, yielding a slightly higher effective moment. The obtained effective moment for $EuNiO_3$ is $5.5\mu_B$, for the 220–320 K temperature range, which will imply a local magnetic moment of the Eu site around $4.7\mu_B$ (assuming $1.73\mu_B$ for low-spin Ni^{3+}), which could be considered as not unreasonable. Also, the broad bump in the magnetic susceptibility in the temperature range between 50 K and 180 K, could be related to a different population (temperature and local-field dependent) of the J levels.

In order to detect the T_N of this compound, we also performed measurements of AC susceptibility around the expected ordering temperature at different excitation frequencies. Only the data at 5 kHz showed a weak peak in the real part of the magnetic susceptibility around 197 K, which we identify as T_N (upper inset of Fig. 5).

Moreover, the magnetic field dependence of the magnetization up to 5 T shows a linear behavior below T_N, indicating the antiferromagnetic character of the magnetic ordering, as shown in Fig. 6. Only the low temperature (1.8 K) hysteresis loop shows a rather weak curvature, probably related to a weak magnetic polarization on the Eu^{3+} ions.

In order to ascertain more clearly the antiferromagnetic ordering temperature (T_N) in $EuNiO_3$, we prepared a compressed pellet (1 Ton) from the powder sample to be able to measure the specific heat in a wide range of temperatures and applied magnetic fields. Fig. 7 displays the specific heat at 0 and 9 T of the externally applied field.

The specific heat of $EuNiO_3$ shows a clear peak close to 200 K, indicating the magnetic phase transition temperature, T_N. However, in this temperature range, we have an important contribution to the specific heat coming from the lattice vibrations. A simple approach of this lattice component can be estimated by the approximation of three harmonic oscillators, sited at different frequencies. The calculation of three harmo-
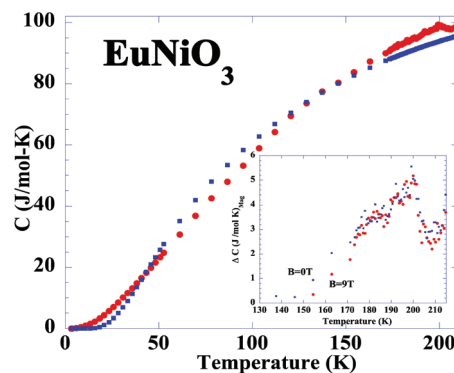

Fig. 7 Temperature dependence of the specific heat (red circles) and a simple calculation with three harmonic oscillators (blue squares). The inset shows the differential specific heat (magnetic component) after the subtraction of the model with 3 oscillators from the experimental measurements at two applied magnetic fields ($B = 0$ and 9 T).

nic oscillators at frequencies equivalent to 160 K, 250 K and 580 K, is shown in Fig. 7 as blue squares. This calculation is able to reproduce well a temperature range between 100 K up to 250 K, where the contribution to the specific heat is considered to come only from the lattice vibration and magnetic ordering. For low temperatures, this simple model is not valid, due to additional components to the specific heat (electronic and crystal field levels). By a direct subtraction of the experimental data from this calculation, we indeed obtain a rather good approximation of the magnetic-only specific heat of this compound ($EuNiO_3$) for the temperature range between 120 K to 230 K. The magnetic component of specific heat is presented in the inset of Fig. 7, showing a clear delta-like transition around the ordering temperature ($T_N = 197$ K). Moreover, upon repeating the same measurement under a strong applied magnetic field of 9 T, with the same calculation of the lattice contribution (the same three harmonic oscillators at the same frequencies), the obtained results are similar, indicating that the magnetic transition is not dependent on the applied magnetic field, thus confirming a pure antiferromagnetic character.

The joint analysis of the magnetization and specific heat data indicates that the $EuNiO_3$ system undergoes antiferromagnetic ordering at $T_N = 197$ K, and at low temperatures there is a very weak polarization by the applied magnetic field on the Eu ions. Moreover, the abrupt contraction of the b parameter of this perovskite in the 175–200 K range, coincident with the onset of the antiferromagnetic ordering, suggests a magnetoelastic coupling, not described so far in rare-earth nickelates.

The magnetic susceptibility of $GdNiO_3$ is displayed in Fig. 8. In principle, the magnetic susceptibility shows a simple behavior with a rather high value of ~1 emu mol^{-1} at low temperatures, without any clear anomaly at any temperature, as probably the susceptibility is dominated by the high magnetic moment of the Gd^{3+} ions. The magnetic ordering temperature of this compound is reported as $T_N = 185$ K.[7] The linear behavior (see the lower inset of Fig. 8) of the inverse of
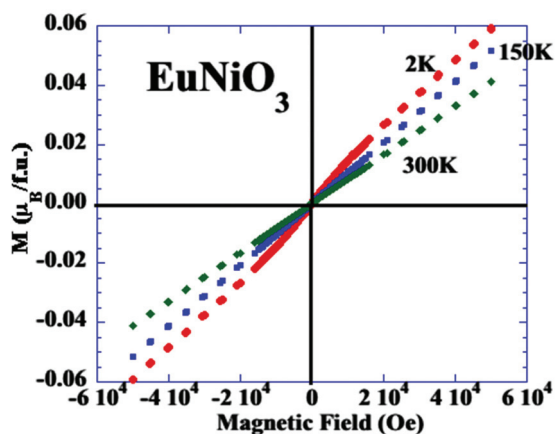

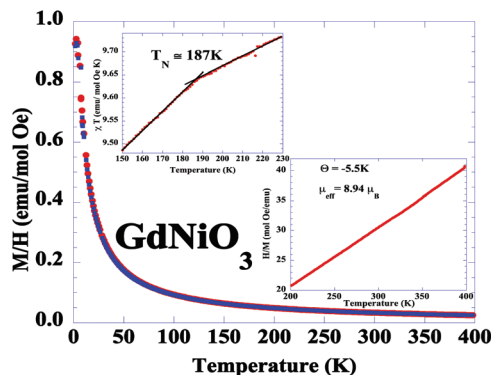Fig. 6 Magnetic field dependence of the magnetization in $EuNiO_3$ at different temperatures.

Fig. 8 Temperature dependence of the magnetic susceptibility of GdNiO$_3$. The upper inset shows the detail of χT in the temperature range around T_N. The lower inset shows the temperature dependence of the inverse magnetic susceptibility in the paramagnetic range.

the magnetic susceptibility in the paramagnetic regime ($T >$ 200 K) implies a paramagnetic moment of almost $9\mu_B$ per f.u. (including Gd and Ni ions) and a Weiss temperature of $\theta = -5.5$ K, indicating the presence of rather weak antiferromagnetic interactions in the paramagnetic phase.

In order to explore the ordering temperature for the Ni sublattice, the plot of χT *vs*. T is enlightening; this curve presents a clear change in the slope at $T_N = 187$ K. This behavior is totally consistent with that reported from the specific heat data, showing that the antiferromagnetic ordering of GdNiO$_3$ occurs at $T_N = 185$ K.[7]

Moreover, the magnetic field dependence of the magnetization is presented in Fig. 9. The initial measurements up to 5 T and low temperature (2 K) of the hysteresis loops seem to indicate an initial process of saturation of the magnetization, but rather incomplete. We performed a second measurement up to higher magnetic fields (14 T), where a complete saturation is observed with a rather high ordered moment of $7.5\mu_B$ per f. u., for magnetic fields higher than 7 T. However, for temperatures below and above the $T_N = 187$ K, a linear behavior,
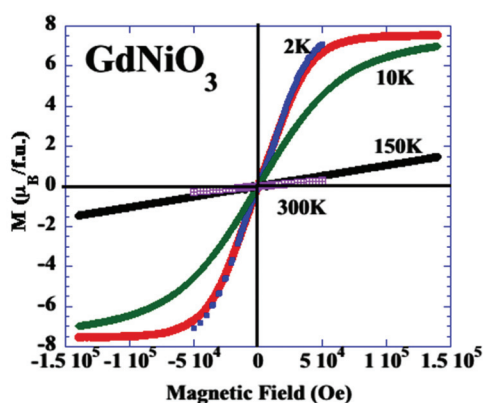

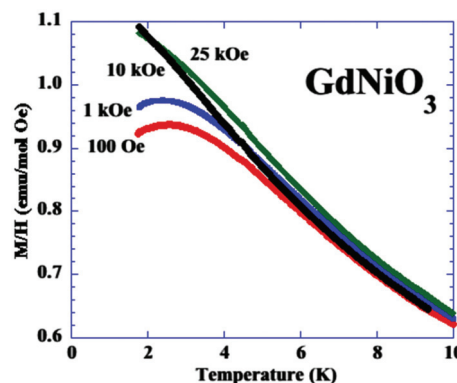**Fig. 9** Hysteresis loops for GdNiO$_3$ at different temperatures with applied magnetic fields up to 14 T.

Fig. 10 Low-temperature dependence of the magnetic susceptibility of GdNiO$_3$, measured at different applied fields from 100 Oe up to 25 kOe.

similar to that expected for an antiferromagnetic system, is clearly observed.

We could conclude that some type of ferromagnetic-like saturation at high magnetic fields is observed in GdNiO$_3$ at very low temperatures ($T < 10$ K), mostly related to the Gd^{3+} ions. In order to clarify this point, we performed detailed measurements of the magnetic susceptibility at low temperatures, for different applied fields, as represented in Fig. 10.

Clearly, the low-temperature magnetic susceptibility shows a maximum close to 2.7 K for small applied magnetic fields (100 Oe). When the magnetic field increases, this maximum is displaced and it finally disappears for higher magnetic fields ($B > 5$ kOe). The data of the hysteresis loops and the magnetic susceptibility at low temperatures and at different applied fields seem to indicate that the Gd sublattice, with an important magnetic moment per ion (around $8\mu_B$), is polarized by the external magnetic field, but an actual long-range ordering of the Gd sublattice is not achieved above 1.75 K.

Conclusions

The evolution of the crystal structures across the MI transitions in EuNiO$_3$ and GdNiO$_3$ has been analyzed for the first time using high-angular resolution synchrotron X-ray diffraction. For YNiO$_3$, utilized as a reference compound, a monoclinic $P2_1/n$ structure is identified by certain reflection splitting in the diffraction patterns in the insulating phase, at RT. In contrast, in the Eu and Gd perovskites, there is no apparent reduction in symmetry from the orthorhombic superstructure defined in the *Pbnm* space group. Therefore, this orthorhombic model has been successfully used to define the crystal structures in the whole temperature range of measurements. The characteristic evolution of the unit-cell parameters, including a conspicuous reduction in volume upon metallization, is observed for both samples; additionally, for EuNiO$_3$ an anomaly in the *b*-axis evolution coincident with T_N suggests a previously unobserved magneto-elastic coupling upon the establishment of the Ni antiferromagnetic structure. The Néel temperature for EuNiO$_3$, previously determined from muon-

spin-rotation experiments and neutron scattering in isotopically enriched samples, is now established at T_N = 197 K from AC susceptibility, assessed with specific heat measurements. For GdNiO$_3$, the ordering of Ni spins is established at T_N = 187 K; the magnetic structure becomes fully polarized, including Gd moments, for external magnetic fields above 7 T.

Conflicts of interest

There are no conflicts to declare.

Acknowledgements

References

1 E. Dagotto, *Science*, 2005, **309**, 257 LP – 262.

2 J. B. Goodenough, *Rep. Prog. Phys.*, 2004, **67**, 1915–1993.

3 H. Kobayashi, S. Ikeda, Y. Yoda, N. Hirao, Y. Ohishi, J. A. Alonso, M. J. Martinez-Lope, R. Lengsdorf, D. I. Khomskii and M. M. Abd-Elmeguid, *Phys. Rev. B: Condens. Matter Mater. Phys.*, 2015, **91**, 1–9.

4 J. A. Alonso, M. J. Martínez-Lope, M. T. Casais, M. A. G. Aranda and M. T. Fernández-Díaz, *J. Am. Chem. Soc.*, 1999, **121**, 4754–4762.

5 M. L. Medarde, *J. Phys.: Condens. Matter*, 1997, **9**, 1679.

6 J. A. Alonso, M. J. Martínez-Lope and I. Rasines, *J. Solid State Chem.*, 1995, **120**, 170–174.

7 J. A. Alonso, M. J. Martínez-Lope, M. T. Casais, J. L. Martínez, G. Demazeau, A. Largeteau, J. L. García-Muñoz, A. Muñoz and M. T. Fernández-Díaz, *Chem. Mater.*, 1999, **11**, 2463–2469.

8 J. L. Garcia-Munoz, J. Rodriguez-Carvajal, P. Lacorre and J. B. Torrance, *Phys. Rev. B: Condens. Matter Mater. Phys.*, 1992, **46**, 4414.

9 J. Torrance, P. Lacorre, A. Nazzal, E. Ansaldo and C. Niedermayer, *Phys. Rev. B: Condens. Matter Mater. Phys.*, 1992, **45**, 8209.

10 J. Varignon, M. Bibes and A. Zunger, *Nat. Commun.*, 2019, **10**, 1658.

11 J. A. Alonso, J. L. García-Muñoz, M. T. Fernández-Díaz, M. A. G. Aranda, M. J. Martínez-Lope and M. T. Casais, *Phys. Rev. Lett.*, 1999, **82**, 3871–3874.

12 J. L. García-Muñoz, J. A. Alonso, M. J. Martínez-Lope, M. T. Fernández-Díaz and M. T. Casais, *Phys. Rev. B: Condens. Matter Mater. Phys.*, 2000, **61**, 1756–1763.

13 A. Mercy, J. Bieder, J. Íñiguez and P. Ghosez, *Nat. Commun.*, 2017, **8**, 1677.

14 J. A. Alonso, M. J. Martínez-Lope, I. A. Presniakov, A. V. Sobolev, V. S. Rusakov, A. M. Gapochka, G. Demazeau and M. T. Fernández-Díaz, *Phys. Rev. B: Condens. Matter Mater. Phys.*, 2013, **87**, 1–12.

15 D. J. Gawryluk, Y. M. Klein, T. Shang, D. Sheptyakov, L. Keller, N. Casati, P. Lacorre, M. T. Fernández-Díaz, J. Rodríguez-Carvajal and M. Medarde, *Phys. Rev. B*, 2019, **100**, 205137.

16 V. Bisogni, S. Catalano, R. J. Green, M. Gibert, R. Scherwitzl, Y. Huang, V. N. Strocov, P. Zubko, S. Balandeh, J. M. Triscone, G. Sawatzky and T. Schmitt, *Nat. Commun.*, 2016, **7**, 1–8.

17 J. Shamblin, M. Heres, H. Zhou, J. Sangoro, M. Lang, J. Neuefeind, J. A. Alonso and S. Johnston, *Nat. Commun.*, 2018, **9**, 1–7.

18 J. Varignon, M. N. Grisolia, J. Íñiguez, A. Barthélémy and M. Bibes, *npj Quantum Mater.*, 2017, **2**, 21.

19 M. Medarde, C. Dallera, M. Grioni, B. Delley, F. Vernay, J. Mesot, M. Sikora, J. A. Alonso and M. J. Martínez-Lope, *Phys. Rev. B: Condens. Matter Mater. Phys.*, 2009, **80**, 245105.

20 U. Staub, G. I. Meijer, F. Fauth, R. Allenspach, J. G. Bednorz, J. Karpinski, S. M. Kazakov, L. Paolasini and F. d'Acapito, *Phys. Rev. Lett.*, 2002, **88**, 126402.

21 M. Zaghrioui, A. Bulou, P. Lacorre and P. Laffez, *Phys. Rev. B: Condens. Matter Mater. Phys.*, 2001, **64**, 81102.

22 Y. Bodenthin, U. Staub, C. Piamonteze, M. García-Fernández, M. J. Martínez-Lope and J. A. Alonso, *J. Phys.: Condens. Matter*, 2011, **23**, 36002.

23 J. Rodríguez-Carvajal, S. Rosenkranz, M. Medarde, P. Lacorre, M. T. Fernandez-Díaz, F. Fauth and V. Trounov, *Phys. Rev. B: Condens. Matter Mater. Phys.*, 1998, **57**, 456–464.

24 M. T. Fernández-Díaz, J. A. Alonso, M. J. Martínez-Lope, M. T. Casais and J. L. García-Muñoz, *Phys. Rev. B: Condens. Matter Mater. Phys.*, 2001, **64**, 144417.

25 M. Casais, M. Martínez-Lope, M. A. G. Aranda, J. L. García-Muñoz, J. A. Alonso and M. T. Fernández-Díaz, *Physica B: Condens. Matter*, 2002, **276–278**, 218–221.

26 J. A. Alonso, M. J. Martínez-Lope, M. T. Casais, J. L. García-Muñoz, M. T. Fernández-Díaz and M. A. G. Aranda, *Phys. Rev. B: Condens. Matter Mater. Phys.*, 2001, **64**, 094102.

27 R. Lengsdorf, A. Barla, J. A. Alonso, M. J. Martinez-Lope, H. Micklitz and M. M. Abd-Elmeguid, *J. Phys.: Condens. Matter*, 2004, **16**, 3355–3360.

28 M. Medarde, P. Lacorre, K. Conder, F. Fauth and A. Furrer, *Phys. Rev. Lett.*, 1998, **80**, 2397–2400.

29 F. Serrano-Sánchez, F. Fauth, J. L. Martínez and J. A. Alonso, *Inorg. Chem.*, 2019, **58**, 11828–11835.

30 F. Fauth, R. Boer, F. Gil-Ortiz, C. Popescu, O. Vallcorba, I. Peral, D. Fullà, J. Benach and J. Juanhuix, *Eur. Phys. J. Plus*, 2015, **130**, 160.

31 A. Caytuero, H. Micklitz, F. J. Litterst, E. M. Baggio-Saitovitch, M. M. Abd-Elmeguid and J. A. Alonso, *Phys. Rev. B*, 2006, **74**, 094433.

32 I. Presniakov, A. Baranov, G. Demazeau, V. Rusakov, A. Sobolev, J. A. Alonso, M. J. Martinez-Lope and K. Pokholok, *J. Phys.: Condens. Matter*, 2007, **19**, 36201.